Progress In Electromagnetics Research, Vol. 138, 255–267, 2013

AN EFFICIENT METHOD TO REDUCE THE PEAK TRANSIENT GROUNDING RESISTANCE VALUE OF A GROUNDING SYSTEM

Run Xiong[1], Bin Chen[1, *], Li-Hua Shi[1], Yan-Tao Duan[1], and Guo Zhang[2]

[1]National Key Laboratory on Electromagnetic Environment and Electro-optical Engineering, PLA University of Science and Technology, Nanjing, Jiangsu 210007, China

[2]78479 Department, Chengdu Military Area of PLA, Chengdu, Sichuan 650222, China

Abstract—In this paper, an efficient method is proposed to reduce the peak transient grounding resistance (P-TGR) of a grounding system. By surrounding the lifting line with a material volume, the P-TGR of the grounding system is greatly reduced. The effect of the surrounding volume conductivity and relative permittivity on the P-TGR is also tested. Second, the rectangular surrounding material volume is shielded with a metallic pipe to reduce the P-TGR further. Third, the shielding metallic pipe is connected to the grounding electrode with thin wire, and the effect of the number of the wires on the P-TGR is also analyzed. It is demonstrated that the P-TGR of the grounding system has been reduced significantly.

1. INTRODUCTION

Sensitive electronic components are being increasingly used both in power and communication systems. These components may suffer logic upset or damage at lower levels of induced electromagnetic interference brought about by lightning. A grounding system is often a part of the lightning protection system. When natural lightning strikes, a large current flows from the cloud to the ground. As a result, evaluation of the transient grounding resistance (TGR) of grounding systems in lightning protection systems has attracted considerable attention [1–11]. The finite-difference time-domain (FDTD) method [12–24], which

Received 25 February 2013, Accepted 19 March 2013, Scheduled 21 March 2013

* Corresponding author: Bin Chen (emcchen@163.com).

provides a simple and efficient way of solving Maxwell' equations for a variety of problems, has been widely applied in the transient analysis of grounding system.

As can be seen in [25], it is difficult to reduce the peak transient grounding resistance (P-TGR) value by increasing the number of the grounding electrode or improving the topology of the grounding system at the assumed ground conductivity and permittivity.

To reduce the P-TGR of the grounding system, three approaches have been introduced in this paper to make the lifting line better matched to the grounding system. First, the lifting line is surrounded by a material volume. The sectional area, the conductivity, and the relative permittivity of the surrounding material are varied and the P-TGR is analyzed. Second, the surrounding material volume is shielded with a metallic pipe to reduce the P-TGR further. Third, the metallic pipe is connected with the grounding electrode by thin wire, and the effect of the wire number on the P-TGR is also analyzed. From the numerical analysis of the TGR, it is demonstrated that the P-TGR of the grounding system is reduced significantly with the approaches in this paper.

2. THE TGR CALCULATION

To calculate the TGR, a grounding model is adopted as shown in Figure 1, where earth is used as the return path [25]. A remote

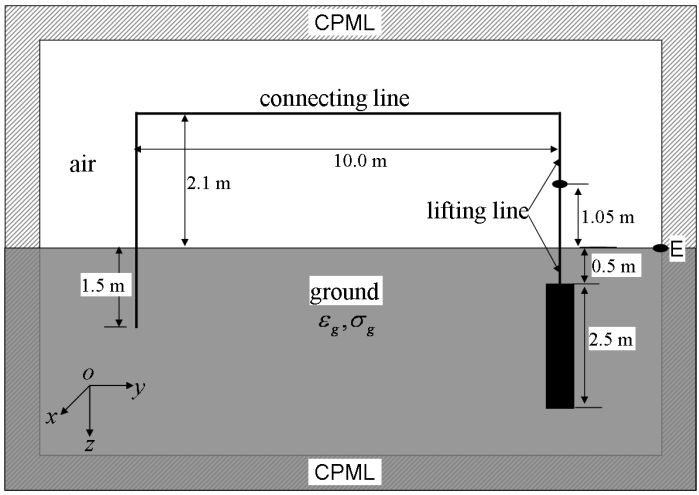

Figure 1. The TGR calculation model.

electrode is used to permit the transient current flowing into the earth. The computational domain is terminated by 8 layer convolution perfectly matched layers [26].

It is assumed that the ground has a constant constitutive parameter, the relative permittivity of the ground is set as $\varepsilon_g = 10.0$, and the conductivity is $\sigma_g = 0.004\,\mathrm{S/m}$. The dimensions of the grounding system are shown in Figure 1. To be simple, a single steel square with the dimensions 250 cm × 5 cm × 5 cm is used as the grounding electrode.

The LEMP is injected 1.05 m above the ground, which can be modeled by

$$E(t) = kE_p(e^{-\alpha t} - e^{-\beta t}) \tag{1}$$

where $k = 1.1016$, $E_p = 5.0 \times 10^4\,\mathrm{V/m}$, $\alpha = 3.7618 \times 10^4\,\mathrm{s}^{-1}$, and $\beta = 1.13643 \times 10^7\,\mathrm{s}^{-1}$. The rise time (10%–90%) of the pulse is 0.2 µs and the fall time (90%–10%) is 58 µs. The power (99.94%) is mainly under the frequency 10 MHz.

The TGR is defined as a ratio of the transient voltage to the transient current

$$R_t = V_t/I_t \tag{2}$$

Here I_t is the transient current flowing through the grounding conductor, which can be defined from the Ampere's Law

$$\begin{aligned} I_t = &\left[H_z\left(i_0 - \frac{1}{2}, j_0 - \frac{1}{2}, k_0\right) - H_z\left(i_0 + \frac{1}{2}, j_0 - \frac{1}{2}, k_0\right)\right]\Delta_z \\ &+ \left[H_x(i_0, j_0 - \frac{1}{2}, k_0 + \frac{1}{2}) - H_x\left(i_0, j_0 - \frac{1}{2}, k_0 - \frac{1}{2}\right)\right]\Delta_x \end{aligned} \tag{3}$$

where $N_0(i_0, j_0, k_0)$ is the point on the lifting line 1.0 m above the source injected point. It is worth noting that the transient current at the point N_0 is chosen because it is difficult to get the current at the point where the lifting line enters the ground.

By integrating the electric field along the air-ground interface from the lifting line to the computational domain boundary (line E of Figure 1), the transient voltage can be obtained:

$$V_t = \sum_{k=N_l}^{N_e} V_k = -\sum_{k=N_l}^{N_e} E_k \Delta s_k \tag{4}$$

where N_l and N_e are the FDTD mesh index of the point where the lifting line enters underground and the point E of Figure 1, respectively. The voltage integrating path length is 4.0 m is this paper.

To model the area near the lifting line and grounding electrode accurately, fine grids are needed in the domain adjacent to the lifting

line and grounding electrode. However, a fine grid of the whole domain would result in incredible computational memory usage, thus the non-uniform standard FDTD method [27] is used near the lifting line area in the x and z direction while a uniform grid is used in the y direction.

A uniform grid is used for the main areas, where the grid size is $\Delta_x \times \Delta_y \times \Delta_z = 10\,\text{cm} \times 10\,\text{cm} \times 10\,\text{cm}$. The expansion factor is set as $\alpha_x = \alpha_z = 1.162$ and a 20 layers non-uniform grid is used, which results in the grid dimension varing from 10 cm to $\Delta_{\min} = 0.5\,\text{cm}$ in the x and z direction for the lifting line areas. The time step is $\Delta t = \Delta_{\min}/2c$, where c is the speed of the light in the free space.

3. PROGRAMS OF REDUCING THE P-TGR

To reduce the P-TGR of the grounding system at the assumed ground conductivity and permittivity, three approaches has been introduced, as shown in Figure 2. Using these approaches, the lifting line is better matched to the grounding system and the P-TGR is therefore decreased.

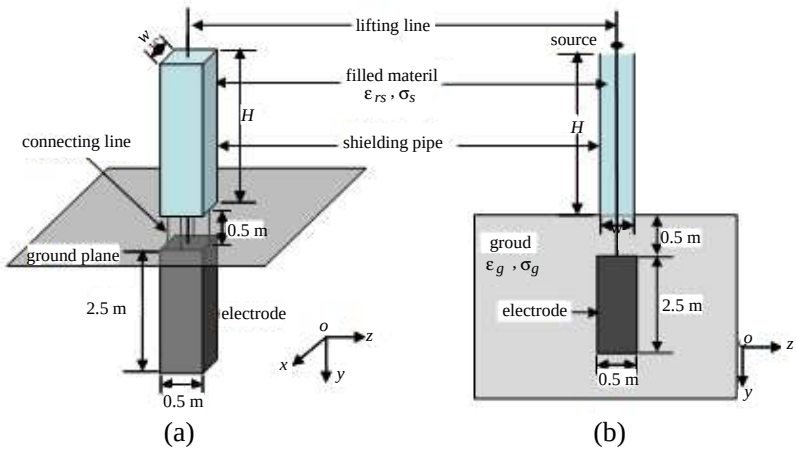

Figure 2. The approaches occupied to reduce the P-TGR.

First, the lifting line is surrounded by a rectangular material volume of varied conductivity and permittivity and the TGR is analyzed. The height of the rectangular surrounding material is H and the width is w. The effect of the surrounding volume size, the conductivity, and the relative permittivity of the surrounding volume on the TGR is analyzed respectively. It is worth to noting that the lifting line is at the center of the surrounding material.

Second, the material volume which surrounds the lifting line is shielded by a metallic pipe. The pipe is a square pipe, which contacts the surrounding material sufficiently, and the height and width of the pipe are the same as the surrounding material. The depth of the shielding pipe is neglected and a perfect electric conductor (PEC) is used in the numerical simulation.

Third, the shielding pipe is connected to the grounding electrode. The lines connect the shielding pipe and the grounding electrode at the middle point of the four sides of the two conductors. The effect of the number of the connecting line on the TGR is also tested.

3.1. The Lifting Line Surrounding Material

In this part, only a material volume is chosen to surround the lifting line, and there is no pipe shielding or line connecting the pipe and the grounding electrode. For simplicity in the rectangular coordinate system, both the lifting line surrounding material volume and the metallic pipe are of the rectangular shape in this work.

First, the surrounding volume size effect on the TGR is analyzed. The conductivity of the surrounding material is $\sigma_s = 0.04\,\mathrm{S/m}$ and the relative permittivity is $\varepsilon_{rs} = 10$. The width of the rectangular material volume w is varied from 2 cm to 10 cm when $H = 1.0\,\mathrm{m}$, and the TGR is calculated as shown in Figure 3(a). The P-TGR of these conditions

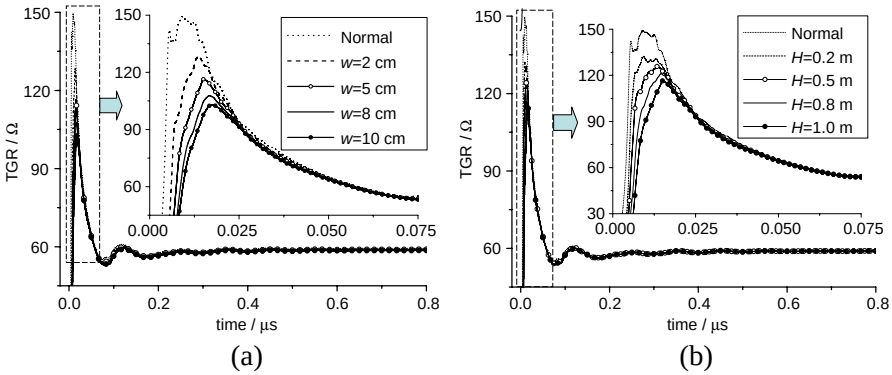

Figure 3. The TGR of the grounding system at varied surrounding volume parameters, where "Normal" indicates the TGR of the grounding system without surrounding volume, shielding pipe or wires. The small graph at the top right corner is the amplified TGR near the peak TGR value. (a) The TGR at varied width of the surrounding volume when $H = 1\,\mathrm{m}$. (b) The TGR at varied height of the surrounding volume when $w = 5\,\mathrm{cm}$.

is listed in Table 1. The surrounding volume height is varied from 0.2 m to 1.0 m when $w = 5$ cm, and the TGR is shown in Figure 3(b).

Table 1. P-TGR of the grounding system versus the surrounding volume width.

w (cm)	0	2	5	8	10
P-TGR (Ω)	149.3	128.3	116.5	107.7	103.0

It can be seen from Figure 3 and Table 1 that increase of the sectional area or the height of the surrounding volume can be efficient to reduce the P-TGR of the grounding system. The P-TGR time is delayed when the lifting line is surrounded by the volume. The TGR is nearly the same after 0.05 μs, which implies that this approach is unable to reduce the constant resistance of the grounding system. Table 1 shows the P-TGR of the varied surrounding volume width. We can see that the reduction effect of enlarging the sectional area of the surrounding volume steadily decreases as the width increases.

Second, the effect of the conductivity of the surrounding material is analyzed. The dimensions of the surrounding material are $L \times w \times w = 100.\ 0\,\text{cm} \times 5.0\,\text{cm} \times 5.0\,\text{cm}$ and the relative permittivity of the surrounding material is $\varepsilon_{rs} = 10$. The conductivity of the surrounding material is increased from 0.004 S/m to 0.1 S/m and the TGR of the grounding system is graphed in Figure 4. It can be seen that the P-TGR of the grounding system is reduced to 126.3 Ω when the material

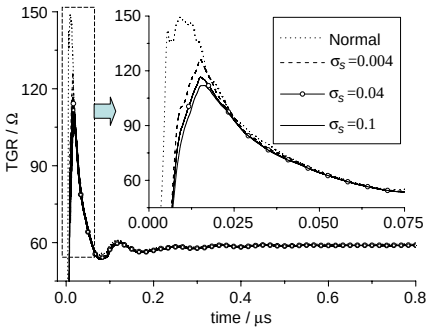

Figure 4. The TGR of the grounding system versus time when the conductivity of the surrounding material varied, where the TGR of the normal condition is also listed for comparison.

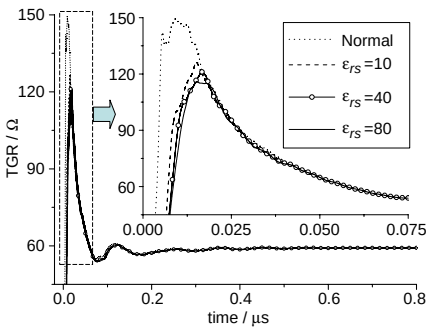

Figure 5. The TGR of the grounding system versus time when the permittivity of the surrounding material varied, where the TGR of the normal condition is also listed for comparison.

of conductivity $\sigma_s = 0.004\,\mathrm{S/m}$ is used to surround the lifting line, compared with $149.3\,\Omega$ when nothing is done. Furthermore, the P-TGR is reduced to $116.4\,\Omega$ and $111.9\,\Omega$ respectively as the conductivity σ_s increases to $0.04\,\mathrm{S/m}$ and $0.1\,\mathrm{S/m}$.

Third, the surrounding material relative permittivity effect on the P-TGR reduction is also studied. The dimension of the surrounding area is $L \times w \times w = 100.0\,\mathrm{cm} \times 5.0\,\mathrm{cm} \times 5.0\,\mathrm{cm}$, and the conductivity of the surrounding material is $\sigma_s = 0.004\,\mathrm{S/m}$. The relative permittivity of the surrounding material is varied from $\varepsilon_{rs} = 10$ to $\varepsilon_{rs} = 80$, and the TGR of the grounding system is graphed in Figure 5. It can be seen that the P-TGR of the grounding system is reduced to $126.3\,\Omega$ when the surrounding material relative permittivity is $\varepsilon_{rs} = 10$, compared with $149.3\,\Omega$ for normal conditions. The P-TGR is further reduced to $121.1\,\Omega$ and $116.0\,\Omega$ respectively when the relative permittivity is increased to $\varepsilon_{rs} = 40$ and $\varepsilon_{rs} = 80$.

From the numerical analysis in this part, it can be seen that the increase of the sectional area, conductivity, and relative permittivity of the lifting line surrounding material volume are all effective ways of reducing the P-TGR. In the analysis below, we fix the dimensions of the rectangular surrounding material volume to $L \times w \times w = 100.0\,\mathrm{cm} \times 5.0\,\mathrm{cm} \times 5.0\,\mathrm{cm}$, the conductivity to $\sigma_s = 0.04\,\mathrm{S/m}$, and the relative permittivity to $\varepsilon_{rs} = 10$.

3.2. The Shielding Pipe

In this part, a rectangular pipe is used to shield the surrounding material volume, but the pipe is not connected with the grounding electrode. The dimensions of the shielding pipe are the same as the lifting line surrounding volume, and the pipe contacts the surrounding material sufficiently. The depth of the shielding pipe is neglected and the PEC boundary is used in the numerical simulation to simulate the pipe.

As graphed in Figure 6, it is clear that the P-TGR is decreased to $102.6\,\Omega$ when the shielding pipe is used, compared with $116.5\,\Omega$ when just a rectangular material volume is used to surround the lifting line. Thus we can say that the shielding pipe is an efficient way of reducing the P-TGR of the grounding system.

3.3. Connecting the Pipe with the Grounding Electrode

In this part, the shielding pipe of the surrounding material volume and the grounding electrode are connected by thin wires at the middle point of the four sides. The lengths of the wires are all 0.5 m. Two conditions are tested here. First, the shielding pipe and the grounding electrode

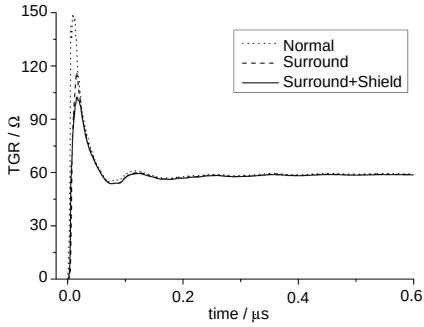

Figure 6. The TGR of the grounding system versus time when the surrounding material volume is connected with the grounding electrode, where "Surround" indicates the condition the lifting line is just surrounded but no pipe are used.

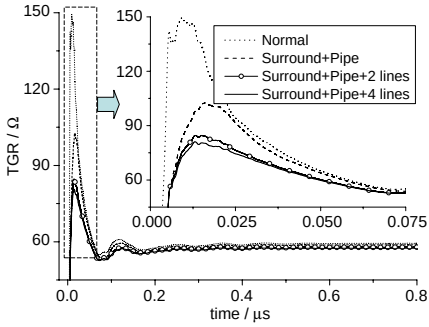

Figure 7. The TGR of the grounding system versus time when the pipe and the grounding electrode are connected, where "Surround + Pipe" indicate the TGR of the case when the surrounding volume is shielded by a pipe but no line are used to connect the pipe and the grounding electrode.

are connected by two thin wires at the face-to-face side. Second, four wires are used to connect the grounding electrode and the shielding pipe at the four sides of the pipe and the TGR of the two conditions are calculated respectively.

Figure 7 graphs the TGR of the two conditions, where the TGR of the normal condition and no line are also graphed for comparison. It can be seen that the P-TGR is reduced from 102.6 Ω to 84.5 Ω when two lines are used, and there is a further 3.5 Ω P-TGR reduction when four lines are used.

Additionally, the electric field which is one cell away from the grounding electrode is also monitored as shown in Figure 8, where "Normal" indicates the field without any approaches and "Proposed" indicates the electric field when the three approaches of this paper is applied to the grounding system. It can be seen that there is a significant decrease of the electric field when the proposed approaches are applied.

From the analysis in this part, it can be concluded that connecting the shielding pipe and the grounding electrode is an efficient way of reducing the P-TGR.

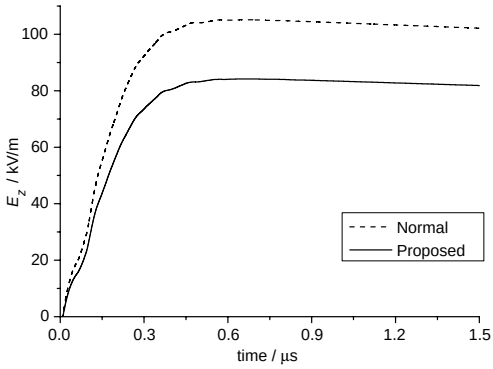

Figure 8. The electric fields near the grounding electrode.

3.4. Validation of the Proposed Approaches to Earthing Grids

To check if the approaches work when earthing grids is involved, the approaches are applied to earthing grids combined with vertical electrodes as shown in Figure 9(a), where the dimension of the grounding system is also shown. The parameters of the surrounding volume and the shielding pipe are the same as above, and four lines are used to connect the shielding pipe with the grids of the grounding system.

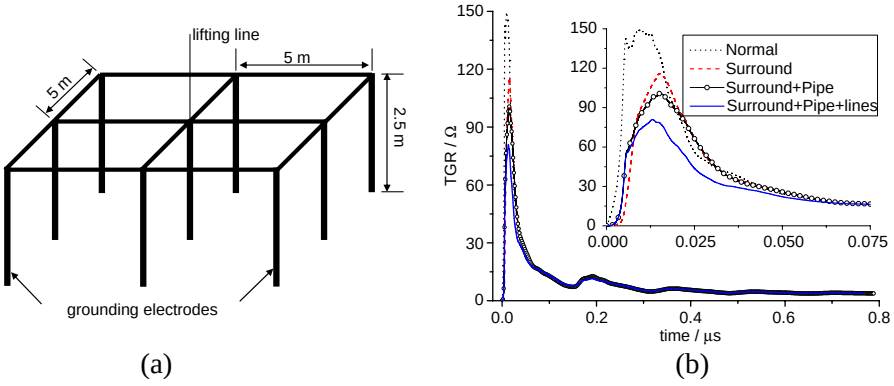

Figure 9. The earthing grids performance with the proposed approaches. (a) Earthing grids combined with vertical electrodes. (b) Reduction of P-TGR of the earthing grids with the proposed approaches.

Figure 9(b) graphs the TGR of the grounding system when the approaches above are applied. It can be seen that the P-TGR of the grounding system is reduced from 150 Ω to 116 Ω when the material volume is used to surround the lifting line. The P-TGR is reduced to 100 Ω when a shielding pipe is occupied, and further reduced to 81 Ω when the shielding pipe is connected to the earthing grids by four lines.

4. CONCLUSIONS

In this work, an efficient method has been proposed to reduce the peak transient grounding resistance (P-TGR) of a grounding system through three steps.

First, a rectangular material volume is occupied to surround the lifting line and it is demonstrated that the P-TGR of the grounding system is further reduced as the sectional area of the surrounding material volume increases. Additionally, an increase of the conductivity and the relative permittivity can decrease P-TGR furthermore.

Second, a metallic pipe is used to shield the lifting line surrounding material volume and it is found that the P-TGR of the grounding system is greatly reduced.

Third, the shielding pipe is connected with the grounding conductor by thin wires. It is demonstrated that the connecting wire can reduce the P-TGR significantly and the reduction effect increases as the number of the wires increases.

From the numerical validation, it is demonstrated that the proposed method in this paper is an efficient way of reducing the P-TGR of the grounding system, and the P-TGR is reduced from 149.3 Ω to 81.0 Ω by using the approaches above. Furthermore, a further P-TGR reduction can be achieved by enlarging the surrounding area or increasing the conductivity or relative permittivity of the surrounding material volume.

REFERENCES

1. IEC 62305-3, Ed. 1, "Protection against lightning — Part 3: Physical damage to structures and life hazard," 2004.
2. Visacro, S. and R. Alipio, "Frequency dependence of soil parameters: Experimental results, predicting formula and influence on the lightning response of grounding electrodes," *IEEE Trans. on Power Delivery*, Vol. 27, No. 2, 927–935, 2012.
3. Zeng, R., J. L. He, Y. Q. Gao, J. Zou, and Z. C. Guan, "Grounding resistance measurement analysis of grounding system in vertical-

layered soil," *IEEE Trans. on Power Delivery*, Vol. 19, No. 4, 1553–1559, 2004.

4. Meliopoulos, A. P. S., S. Patel, and G. J. Cokkinides, "A new method and instrument for touch and step voltage measurement," *IEEE Trans. on Power Delivery*, Vol. 9, No. 4, 1850–1860, Oct. 1994.
5. Tsumura, M., Y. Baba, N. Nagaoka, and A. Ametani, "FDTD simulation of a horizontal grounding electrode and modeling of its equivalent circuit," *IEEE Trans. on Electromagnetic Compatibility*, Vol. 48, No. 4, 817–825, 2006.
6. Gomes, C. and Z. A. Zb. Kadir, "Protection of naval systems against electromagnetic effects due to lightning," *Progress In Electromagnetics Research*, Vol. 113, 333–349, 2011.
7. Izadi, M., M. Z. A. Ab Kadir, and C. Gomes, "Evaluation of electromagnetic fields associated with inclined lightning channel using second order FDTD-Hybrid Methods," *Progress In Electromagnetics Research*, Vol. 117, 209–236, 2011.
8. Izadi, M., M. Z. A. Ab Kadir, and C. Gomes, "Evaluation of lightning current and velocity profiles along lightning channel using measured magnetic flux density," *Progress In Electromagnetics Research*, Vol. 130, 473–492, 2012.
9. Izadi, M., M. Z. A. Ab Kadir, C. Gomes, and V. Cooray, "Evaluation of lightning return stroke current using measured electromagnetic fields," *Progress In Electromagnetics Research*, Vol. 130, 581–600, 2012.
10. Izadi, M., M. Z. A. Ab Kadir, C. Gomes, and W. F. W. Ahmad, "An analytical second-FDTD method for evaluation of electric and magnetic fields at intermediate distances from lightning channel," *Progress In Electromagnetics Research*, Vol. 110, 329–352, 2010.
11. Gomes, C. and M. Z. A. Ab Kadir, "Protection of naval systems against electromagnetic effects due to lightning," *Progress In Electromagnetics Research*, Vol. 113, 333–349, 2011.
12. Taflove, A. and S. C. Hagness, *Computational Electrodynamics: The Finite-difference Time-domain Method*, 3rd Edition, Artech House, 2005.
13. Lee, K. H., I. Ahmed, R. S. M. Goh, E. H. Khoo, E. P. Li, and T. G. G. Hung, "Implementation of the FDTD method based on Lorentz-Drude dispersive model on GPU for plasmonics applications," *Progress In Electromagnetics Research*, Vol. 116, 441–456, 2011.
14. Kong, Y.-D. and Q.-X. Chu, "Reduction of numerical dispersion of

the six-stages split-step unconditional-stable FDTD method with controlling parameters," *Progress In Electromagnetics Research*, Vol. 122, 175–196, 2012.

15. Sirenko, K., "An FFT-accelerated FDTD scheme with exact absorbing conditions for characterizing axially symmetric resonant structures," *Progress In Electromagnetics Research*, Vol. 111, 331–364, 2011.
16. Xiao, S.-Q., Z. H. Shao, and B.-Z. Wang, "Application of the improved matrix type FDTD method for active antenna analysis," *Progress In Electromagnetics Research*, Vol. 100, 245–263, 2010.
17. Cao, D.-A. and Q.-X. Chu, "FDTD analysis of chiral discontinuities in waveguides," *Progress In Electromagnetics Research Letters*, Vol. 20, 19–26, 2011.
18. Mao, Y.-F., B. Chen, H.-Q. Liu, J.-L. Xia, and J.-Z. Tang, "A hybrid implicit-explicit spectral FDTD scheme for the oblique incidence programs on periodic structures," *Progress In Electromagnetics Research*, Vol. 128, 153–170, 2012.
19. Ai, X., Y. Han, C. Y. Li, and X.-W. Shi, "Analysis of dispersion relation of piecewise linear recursive convolution FDTD method for space-varying plasma," *Progress In Electromagnetics Research Letters*, Vol. 22, 83–93, 2011.
20. Kong, L.-Y., J. Wang, and W.-Y. Yin, "A novel dielectric conformal FDTD method for computing SAR distribution of the human body in a metallic cabin illuminated by an intentional electromagnetic pulse (IEMP)," *Progress In Electromagnetics Research*, Vol. 126, 355–373, 2012.
21. Kong, Y.-D., Q.-X. Chu, and R.-L. Li, "Study on the stability and numerical error of the four-stages split-step FDTD method including lumped inductors," *Progress In Electromagnetics Research B*, Vol. 44, 117–135, 2012.
22. Xiong, R., B. Chen, Y. Mao, B. Li, and Q.-F. Jing, "A simple local approximation FDTD model of short apertures with a finite thickness," *Progress In Electromagnetics Research*, Vol. 131, 135–152, 2012.
23. Vaccari, A., A. Cala'Lesina, L. Cristoforetti, and R. Pontalti, "Parallel implementation of a 3D subgridding FDTD algorithm for large simulations," *Progress In Electromagnetics Research*, Vol. 131, 135–152, 2012.
24. Xu, K., Z. Fan, D.-Z. Ding, and R.-S. Chen, "GPU accelerated unconditionally stable Crank-Nicolson FDTD method for the analysis of three-dimensional microwave circuits," *Progress In Electromagnetics Research*, Vol. 102, 381–395, 2010.

25. Xiong, R., B. Chen, J.-J. Han, Y.-Y. Qiu, W. Yang, and Q. Ning, "Transient resistance analysis of large grounding systems using the FDTD method," *Progress In Electromagnetic Research*, Vol. 132, 159–175, 2012.
26. Roden, J. A. and S. D. Gedney, "Convolution PML (CPML): An efficient FDTD implementation of the CFS-PML for arbitrary media," *Microwave and Optical Technology Letters*, Vol. 27, No. 5, 334–339, Dec. 2000.
27. Yu, W.-H. and R. Mittra,, "A technique of improving the accuracy of the nonuniform time-domain algorithm," *IEEE Trans. on Microw. Theory Tech.*, Vol. 47, No. 3, 353–356, 1999.